

## THE EFFECTS OF ELECTRON IRRADIATION AND FLUORIDE SALT MELT $ZrF_4 - NaF$ ON MECHANICAL PROPERTIES OF HASTELLOY N TYPE ALLOYS

*V.M. Azhazha, A.S. Bakai, A.N. Dovbnya, K.V. Kovtun, S.D. Lavrinenko,  
D.G. Malykhin, M.M. Pylypenko, V.I. Savchenko, N.A. Semenov,  
S.V. Strygunovsky, B.I. Shramenko, N. Wanderka\**

*National science center "Kharkov Institute of Physics and Technology",  
1 Akademicheskaya St., 61108 Kharkov, Ukraine; E-mail: azhazha@kipt.kharkov.ua;  
\*Hahn-Meitner Institute, Berlin, Germany*

NSC KIPT has cast Hastelloy N type alloys that are to be used in molten-salt reactors (MSR). A study was made on the collective effects of exposure to electron irradiation and melt of sodium and zirconium fluorides at the temperature 650°C for 700 hours on mechanical properties of those alloys.

### 1. INTRODUCTION

Molten-salt reactors (MSR) are promising reactors of the next generation that will be able not only to produce electric power, but also make re-burn and transmutation of the radiation waste [1-3].

The coolant for the MSRs is the melt of fluoride salts of lithium, sodium, zirconium with the addition of fissile material, uranium or plutonium fluoride. The structural materials proposed for the reactors of this type are alloys of the type Hastelloy N and its Russian analog KhN80MT.

On the base of high-purity ingredients, NSC KIPT has cast alloys of this type, fabricated samples for corrosion tests conducted under electron irradiation.

The aim of this work was to make a study on the collective effects of the sodium and zirconium fluoride salt melt and electron irradiation on the mechanical properties of the alloys of the type Hastelloy N.

### 2. MATERIALS AND RESEARCH METHODS

Samples of the alloys (alloys "A" and "B") were cast at NSC KIPT from high-purity initial components in the induction casting facility [4,5]. The composition of the alloy "A" is as follows: Ni-base, Mo – 11.7; Cr – 6.7; Ti – 0.47; Al – 0.83; Fe – 1.5; Mn – 0.5; Si – 0.15 wt.%. In the alloy "B", 0.5 wt. % of niobium was substituted for Cr, 0.05 wt.% of yttrium added. Strips 0.3 mm thick were rolled out of the alloys, from which research samples were cut out with the size 24x28 mm. The smaller side of the sample was oriented along the direction of the rolling. After the rolling the samples underwent the following thermal treatment: annealing in the air at 1100°C for 1 hour with the subsequent quenching in water. With the quenching over, the sample surface was de-scaled and they were annealed in argon atmosphere at the temperature 675°C for 50 hours (ageing). One plate was cut to produce three samples for mechanical tests, using the electric spark cutting. A jumper was fashioned on one of the shoulders of the samples to be

used for the mechanical tests to keep the samples in place on the plate. The layout of sample disposition, as shown in Fig. 1, provides for sufficient irradiation homogeneity in the sample plane.

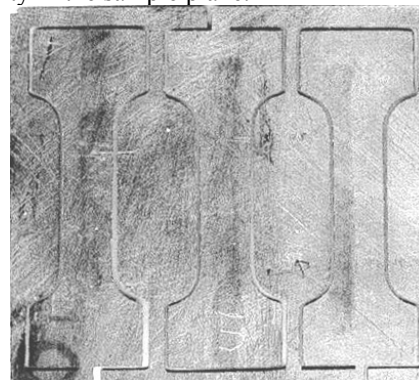


*Fig. 1. Sample disposition for mechanical tests on Hastelloy N plate*

Several such plates were made of the alloys of two compositions. Irradiation samples were mounted in ampoules made of a carbon-carbon composite material. After the sample assembly, zirconium and sodium fluoride melt was poured into the ampoule. The schematic of plate disposition in the irradiation ampoule is given in Fig. 2.

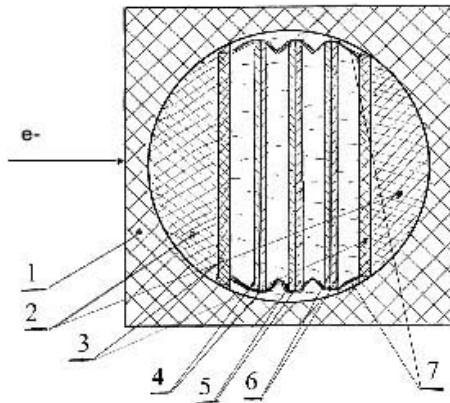


Fig. 2. Schematic layout of plates in ampoule: 1 – ampoule frame; 2 – insets; 3 – C-C composite plate; 4-6 – first, second and third pairs of samples, respectively; 7 – sample mount rig

The sample irradiation was carried out at the dedicated Electron Irradiation Test Facility [6] (EITF) installed at the electron linac output. The EITF setup and disposition of research sample ampoules are given in Fig. 3. The average electron energy during the irradiation was 9.6 MeV, the total average beam current being 520  $\mu$ A. While being irradiated, the samples were kept in the fluoride melt at the temperature 650°C for 700 hours.

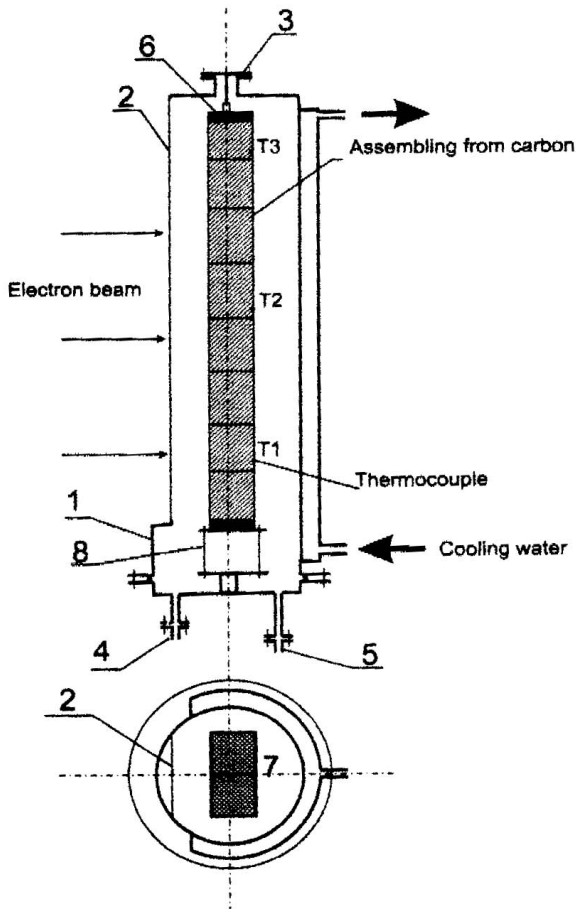


Fig. 3. EITF setup: 1 – stand body, 2 – input window, 3 – sample assembly centering flange, 4 – chamber evacuation vent, 5 – argon puffing vent, 6 – graphite plate, 7 – container assembly, 8 – container assembly holder [6]

The paper [7] reported the results of simulations of the electron beam energy absorption in the ampoule containing the samples that was filled up with sodium and zirconium fluoride melt. The calculated profile of absorbed electron beam energy is shown in Fig. 4.

As one can gather from the above calculations, the first plate (position 4, Fig. 2) and last one (position 6, Fig. 2) of the research Hastelloy-type alloy were irradiated to considerably different doses, 5,066 and 64 eV per atom, respectively. As one can gather from the above calculations, the first plate (position 4, Fig. 2) and last one (position 6, Fig. 2) of the research Hastelloy-type alloy were irradiated to considerably different doses, 5,066 and 64 eV per atom, respectively. After the irradiation, the ampoules with the samples were disassembled mechanically, the samples desalted. To extract sample needed for mechanical tests, it would suffice just to cut off the jumper on the sample shoulder (see Fig. 1).

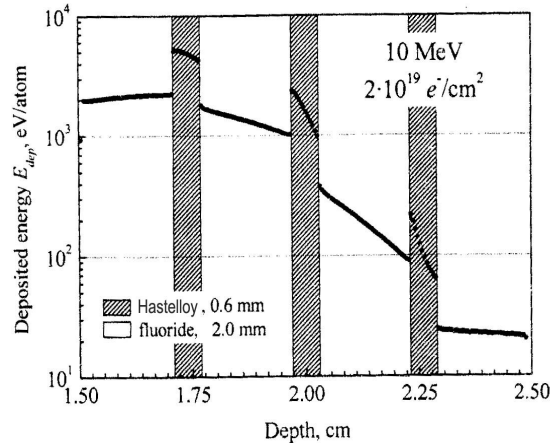


Fig. 4. Calculated profile of absorbed electron beam energy in ampoule containing samples [7]

The irradiation conditions were such that the remnant radioactivity of mechanical test sample should not exceed the value of 0.3  $\mu$ Sv/h. The mechanical tests of the samples were done at a tearing machine of the type 1246P-2/2600 in the temperature interval 20 to 650°C. The sample microstructure was examined in the optical microscope “MMR-4”, microhardness measured at the device PMT-3. The X-ray structural studies on the alloys were made at the device DRON-07, with a scintillation counter absorbing the radiation spectra of  $\text{CuK}\alpha$  and  $\text{CoK}\alpha$ . The filming was made according to the Bragg-Brentano optical scheme.

### 3. EXPERIMENTAL RESULTS AND THEIR DISCUSSION

Studies were made on the mechanical properties and microstructure of the initial samples after the quenching and after the quenching with subsequent ageing. The sample microstructure after rolling, quenching and ageing is given in Fig. 5. The very same figure shows the

microstructure of the mechanical test specimens at the place of rupture. The samples display good plasticity, its grains being slightly elongated at the place of rupture. The mechanical tests were also made of the post-ageing samples in the temperature interval from room one to 600°C. The fracture strength characteristics of the Hastelloy-type alloys (alloys “A” and “B”) at different temperatures are given in Table 1 and in Fig. 6 (shown only for the ultimate strength value).

The tests at elevated temperatures showed a leaping progression of the stress-deformation curve, as one can

see on a part of the recording of the tensile strength diagram given in Fig. 7 (the sample was tested at the temperature 450°C). This kind of behavior of the stress-deformation curves is characteristic of many alloys at elevated temperatures, and it can be accounted for by the dynamic deformation ageing [11,12]. Table 2 gives the results of the sample mechanical tests after the electron irradiation in the melt of zirconium and sodium fluoride salts at the temperature 650°C for 700 hours. The layout of disposition of the samples “A” and “B” and their numeration are given in Fig. 8.

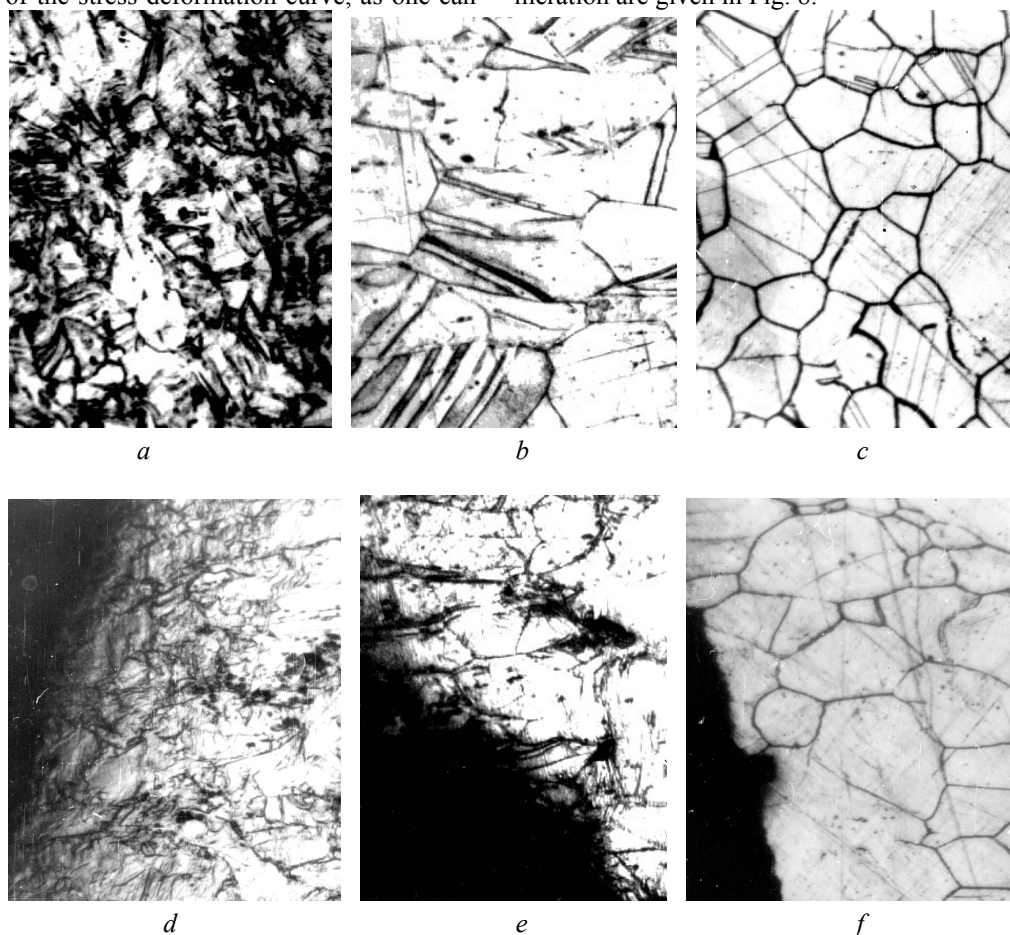


Fig. 5. Structure of initial mechanical test sample (a,b,c) of Hastelloy-type alloy and samples (d,e,f) at the place of rupture: a, d – post-rolling samples; b, e – samples after rolling and quenching; c, f – samples after rolling, quenching and annealing (380 x magnification)

Table 1

Results of mechanical tests of initial samples of alloys “A” and “B” at different temperatures

Parameter	20°C	250°C	400°C	500°C	600°C
Alloy “A”					
$\sigma_B$ , MPa	900	776	710	730	398
$\sigma_{0.2}$ , MPa	396	364	314	336	288
$\delta$ , %	63,5	60,5	62,5	37	14,5
Alloy “B”					
$\sigma_B$ , MPa	845	737,5	713	695	443
$\sigma_{0.2}$ , MPa	397	376,5	339	335,5	310
$\delta$ , %	53	52	44,5	52	19
Alloy KhN80MT (annealing 1100°C + quenching + 100 h ageing 650°C)					
$\sigma_B$ , MPa	765	–	–	632	–
$\sigma_{0.2}$ , MPa	256	–	–	157	–
$\delta$ , %	49,0	–	–	60,9	–

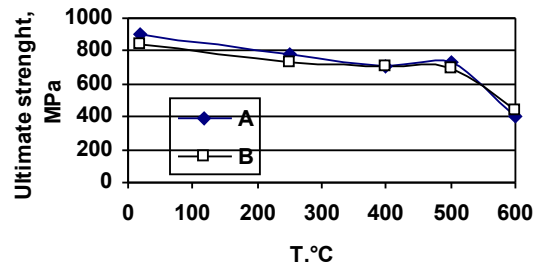


Fig. 6. Dependence of mechanical properties of initial alloys "A" and "B" of Hastelloy type on temperature of testing

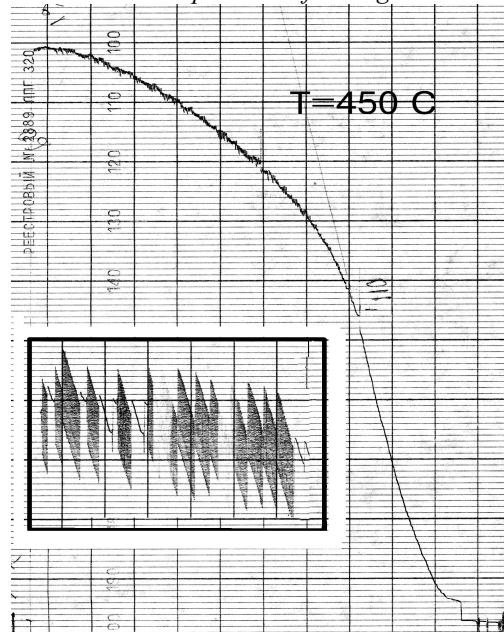
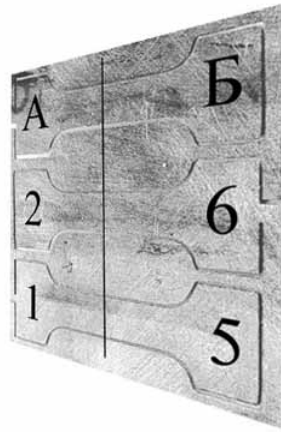


Fig. 7. A fragment of tensile strength diagram of Hastelloy-type alloy sample at the temperature 450°C after corrosion tests for 100 hours. The inset shows the leaping progression on the smaller scale. On the axis of ordinates is shown the stress, on the axis of abscissas, the elongation

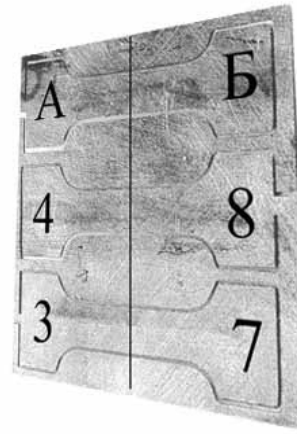
Table 2

**Mechanical characteristics of Hastelloy-type alloy samples after electron irradiation**

Sample condition	T <sub>test</sub> , °C	σ <sub>B</sub> , MPa	σ <sub>0.2</sub> , MPa	δ, %
E <sub>dep</sub> , eV/atom			<b>Alloy "A"</b>	
5,066(sample #1)	20	626	333	35
64(sample #3)		848	576	54
5,066(sample #2)	650	276	213	15
64(sample #4)		362	255	15
Initial non-irradiated	20	900	395	63
	600	397	288	14
Post-corrosion test 650°C, 700 h Non-irradiated	20	1070	875	43
	650	510	440	9
E <sub>dep</sub> , eV/atom			<b>Alloy "B"</b>	
5,066(sample #5)	20	876	412	50
64(sample #7)		851	415	48
5,066(sample #6)	650	293	214	15
64(sample #8)		350	318	15
Initial non-irradiated	20	845	397	53
	600	443	310	19



First sample, irradiation dose 5,066 eV per atom

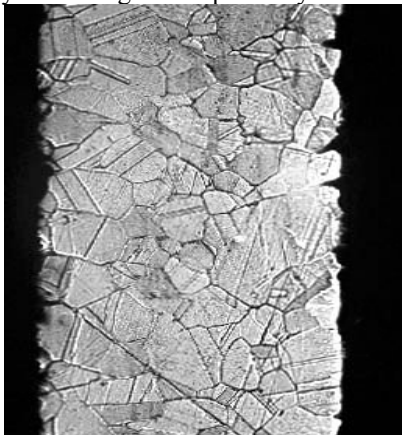


Last sample, irradiation dose 64 eV per atom

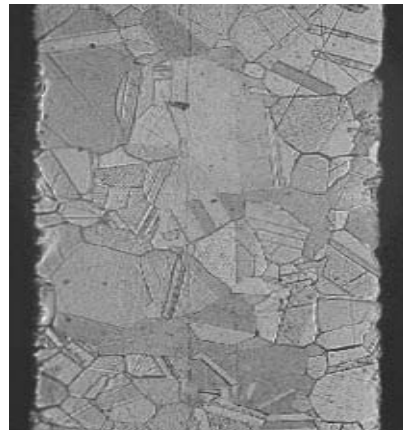
Fig. 8. Disposition layout and numeration of samples of alloys "A" and "B" placed in ampoules to be irradiated

A comparison of the results of the effects of the electron and in-reactor neutron irradiation on the alloys studied [2] indicates that the effects of the electron irradiation are qualitatively similar to those of the neutron irradiation on the alloy of this composition. The lower values of the yield strength and plasticity limit in our

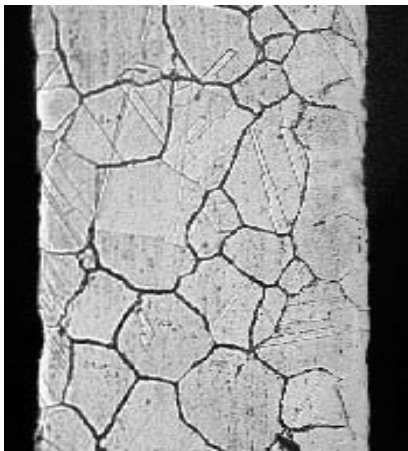
samples can be attributed to the different irradiation conditions and peculiarities of the electron irradiation effects on the chemical kinetics in the fluoride salt melt. The microstructures of the alloys "A" and "B" irradiated to different doses are given in Fig. 9.



Alloy "A". #1 Irradiation dose is 5,066 eV per atom



Alloy "A". #3 Irradiation dose is 64 eV per atom



Alloy "B". #5 Irradiation dose is 5,066 eV per atom



Alloy "B". #7 Irradiation dose is 64 eV per atom

Fig. 9. Microstructure of samples of alloys "A" and "B" after irradiation. Electron beam was directed from the left. The sample width is about 300 microns

One can see that the samples of the alloy "A" are more liable to corrosion than those of the alloy "B". The

microhardness values of alloy samples irradiated to the doses 5,066 and 64 eV/atom are  $H\mu=2860$  MPa for the

samples of the alloy “A” and  $H\mu=3,210, 3,000$  MPa for the samples of the alloy “B”, respectively. The measurement of microhardness along the sample thickness (see Fig. 10) did not reveal any differences between the sample middle and its edges.

The values of nanohardness and moduli of elasticity as measured on the surface and throughout the bulk of the Hastelloy alloys “A” and “B” are given in Table 3 [8].

The nanohardness values in the initial samples are seen to be the same for their surface and bulk. After the samples had been irradiated at the EITF, the sample bulk nanohardness value remained actually unchanged. The post-irradiation surface nanohardness became lower indicating about deterioration of the surface pattern. Examination of the morphology indicated that the samples irradiated to the greater electron dose had a larger number of inter-grain cracks as shown in Fig. 11.

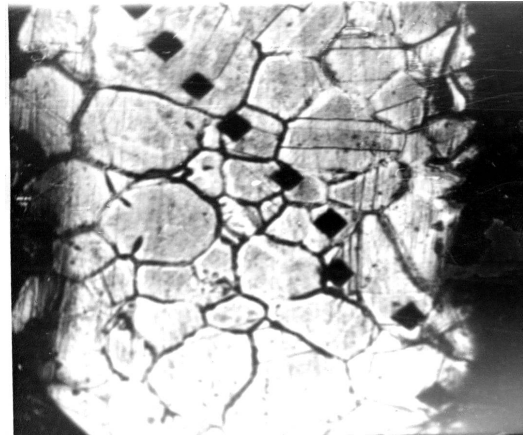


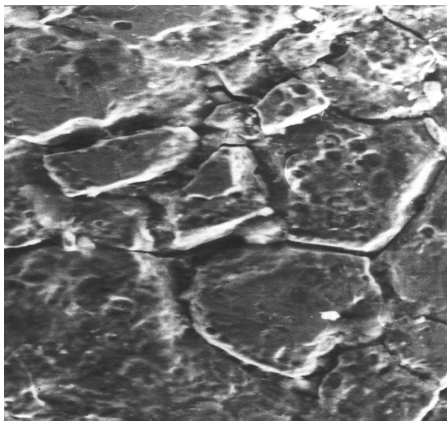
Fig. 10. Microstructure of sample after irradiation in ampoule #7. Electron beam was directed from the left. The sample width is about 300 microns. The squares inside of sample indicate traces of the microhardness measurement

The surfaces of the sample rupture after the mechanical tests display that the destruction occurs mainly along the grain boundaries, although some individual grains were torn plastically (see Fig. 12). The addition of niobium and yttrium solutes to the alloy “B” enhances considerably the mechanical properties of this alloy.

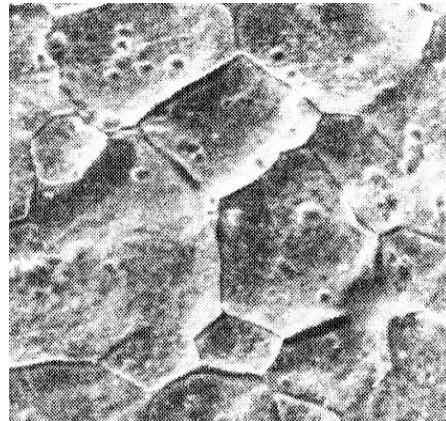
Table 3

Values of nanohardness and moduli of elasticity as measured on the surface and throughout the bulk of the alloys [8]

Material	$E_{dep}$ , eV/atom	$E_{surf}$ , GPa	$E_{bulk}$ , GPa	$H_{surf}$ , GPa	$H_{bulk}$ , GPa
Hastelloy A, initial post-ageing, 50 h at 675°C	0	266±16	266±16	4.7±0.3	4.7±0.3
Hastelloy A, after 700 h at 675°C	0	219	219	3±2.2	6±0.3
	64	242±35	268±8	5.7±0.3	-
	5066	229±35	256±13	5.7±0.5	-
Hastelloy B initial post-ageing, 50 h at 675°C	0	297±11	297±11	6.9±0.3	6.9±0.3
Hastelloy B, after 700 h at 675°C	0	-	-	4±0.5	6.9±0.3
	64	55±30	255±6	2.9±1.7	7.1±0.4
	5066	150±50	255±7	5.5±1.2	6.8±0.2



a



b

Fig. 11. Surface of samples of alloy "A" that had been subjected to electron irradiation: a – sample #2, irradiation dose is 5,066 eV per atom; b – irradiation dose is 64 eV per atom, 950 x magnification

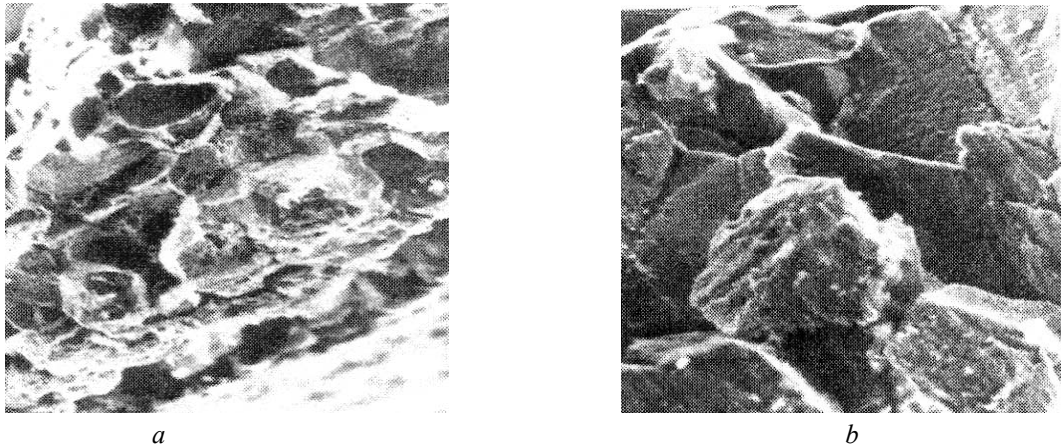


Fig. 12. Surface of samples of alloy "A" that had been subjected to electron irradiation, at the place of rupture, sample #4: a – 625 x magnification; b – 1,425 x magnification

Table 4 gives the results of a study on the phase analysis of samples of the alloys "A" (samples #1, 3) and "B" (samples #5, 7) after the electron irradiation at the temperature 650°C for 700 hours. The phases detected were numbered in the following way: Ni<sub>3</sub>Al(Ti) – 1; NiAl – 2; Ni<sub>2</sub>Al<sub>3</sub> – 3; Ni<sub>3</sub>Mo – 4; NiCr – 5; 7NaF·6ZrF<sub>4</sub> – 6.

In accordance with the results obtained, among the entire phase diversity that is inherent to the alloys sub-

jected to corrosion tests without irradiation, the irradiated samples contain phases in their formed crystalline state only of Ni<sub>3</sub>Mo and remnants of the compound fluoride 7NaF·6ZrF<sub>4</sub>. The phase Ni<sub>3</sub>(Al,Ti) is found only in sample 5 of the alloy "B". Traces of the fluoride are more clearly apparent in samples of the alloy "A" and, especially, in sample 1.

Table 4

Results of phase analysis of samples of alloys "A" and "B" after electron irradiation

D(E)	Phase # (see Table 3)	Line intensity (%)			
		Sample #1 (A)	Sample #3 (A)	Sample #5 (B)	Sample #7 (B)
3.48	3	< 0.5	–	–	–
3.12...3.15	6	4.0	2.0	0.5	0.5
2.86	2,3,(6)	–	1.5	–	–
2.113...2.115	4	1.0	2.0	1.5	–
2.09	1	–	–	1.5	–
2.00...2.02	3,6,(2)	–	< 0.5	–	< 0.5
1.98	4	2.0	–	–	2.0
1.95...1.96	4,6	–	1.0	–	–
1.91...1.92	6	3.5	1.0	–	2.0
1.83...1.84	1	–	< 0.5	1.0	–
1.81	1	–	–	–	–
1.64	6,(2)	2.5	–	–	–
Presence of phases ##		4,6	4,6	1,(4),(6)	(4),6

Figures 13 and 14 show the relations of the ultimate and yield strengths vs. sample ageing at different test temperatures. The ageing went on for up to 50 hours in argon atmosphere, and further on it continued in the fluoride salt melt in the course of the corrosion tests. Separate dots stand for results of the sample mechanical tests

after the irradiation for 700 hours at the temperature 650 °C. The samples were tested at 20 and 650°C (the "first" and "last" labels stand for the position of the samples relative to electron beam path and correspond to irradiation doses 5,066 and 64 eV per atom, respectively).

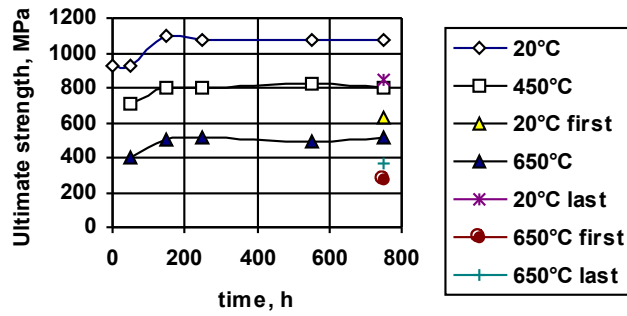


Fig. 13. Dependence of the ultimate strength of samples of the alloy "A" tested at different temperatures on exposure duration in the melt of zirconium and sodium fluoride salts. The "first" and "last" labels stand for the position of the samples relative to electron beam path and correspond to the irradiation doses 5,066 and 64 eV per atom, respectively, the test temperatures being 20 and 650°C

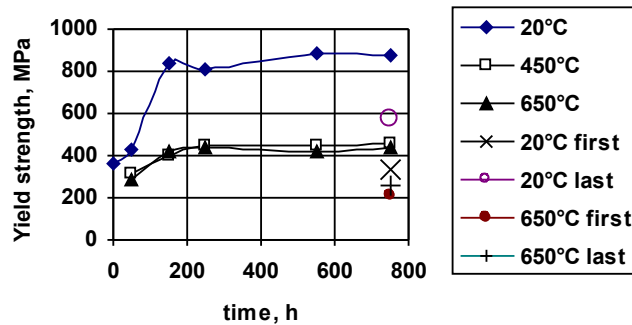


Fig. 14. Dependence of the yield strength of samples of the alloy "A" tested at different temperatures on exposure duration in the melt of zirconium and sodium fluoride salts. The "first" and "last" labels stand for the position of the samples relative to electron beam path and correspond to the irradiation doses 5,066 and 64 eV per atom, respectively, the test temperatures being 20 and 650°C

The main shortcoming of the dispersion-strengthened alloys is their structural instability at the temperatures above  $0.6 T_{\text{melt}}$  that exceed the optimum ageing ones. This instability is due to the fact that the number and composition of the phases as well as their size distribution can vary vs. time [9]. Those variations can be substantial over the sample exposure times exceeding 1,000 hours. The strengthening phase particle sizes in the ageing alloys after the above treatments are mostly of the order 15...20 nm, which, even at a relatively low phase volume content, secures a high strength level owing to the shortness of inter-particle distances and a coherent, or partially coherent, inter-phase boundary.

Fig. 15 shows schematically variation of the yield strength in the course of disintegration of the oversaturated solid solutions [9] when all the stages of formation and growth of the coherent precipitates are realized sequentially: boundary coherence violation stage and precipitate coalescence stages. Normally, the pre-ageing yield strength is equal to that of the oversaturated solid solution. As the ageing progresses, the precipitate volume fraction increases, and, since the particle size is very small, the yield strength increment is approximate-

ly equal to the cube root from the precipitate phase volume content. With evolution of the ageing process, the forming particles begin to coarsen and at some moment lose their coherence with the matrix, the effective precipitate volume fraction beginning to decrease. The yield strength variation is not great (see Fig. 14), remaining actually unchanged upon reaching the exposure time of more than 300 hours. After completion of the second phase precipitation from the solid solution, there occurs the process of coarsening (coalescence) of particles, and, when their size exceeds the critical value  $R = G \cdot b / \sigma_s$ , the yield strength begins to decrease [9], because the matrix frees itself from fine precipitates that hinder the dislocation pile-up.

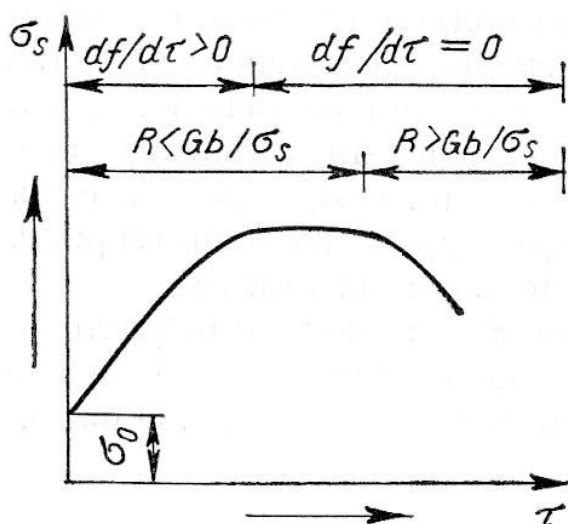


Fig. 15. Typical yield strength dependence during oversaturated solid solution disintegration on ageing time (scheme) [9]:  $R$  – the precipitate particle radius,  $G$  – the matrix shear modulus,  $b$  – the Burgers vector,  $f$  – the second phase volume content,  $\sigma_s$  – the yield strength

In accordance with [10], the kinetics of disperse particle growth at the stage of coalescence during isothermal growth is determined by an equation of the kind  $\bar{r}^3 \sim t$  ( $\bar{r}$  – the mean particle radius,  $t$  – the time), when the phase precipitates from the oversaturated solid solution and the particle volume fraction of the second phase is not taken into account, i.e. at  $f \rightarrow 0$  ( $f$  – the precipitate volume fraction). With increasing of the precipitate volume fraction, the rate of particle coarsening increases as well, obeying the solution-precipitation mechanism, and, in this case, the influence of particle volume fraction on the growth rate constant must be taken into account, using the additional factor  $k(f)$  [11]. The nature of the yield strength curve behavior of samples of the alloy “A” at the test temperatures 450 and 650°C, with the exposure times exceeding 25...800 hours (see Fig. 13, 14), corresponds to such case when only the second phase particle coalescence occurs until the particle size reaches the critical value (see, precipitate growth stage in Fig.15). By comparing the ultimate strength time dependence of the alloy “A”, exposed in the salt melts up to 700 hours, with the typical behavior of this value for disintegrating solid solutions (Fig. 15), one can see that the exposure duration of 700 hours at 650°C corresponds to the early stage of precipitate coalescence. The available experimental data does not permit the straightforward conclusion to be made about the cause of the structural changes entailing a noticeable decrease in the yield strength of the irradiated samples as compared with the non-irradiated ones. From Fig.15 one can see that the cause can be both reduction of the precipitates to fine sizes and their partial dissolution under irradiation and enhancement of the coalescence process. Besides, the corrosion processes violate the surface layer of the samples to the depth of about 20 microns. This causes reduction of the transverse cross-sections of the mechanical test samples and deterioration of their me-

chanical characteristics. Further research is needed for clarification on those problems.

#### 4. CONCLUSIONS

- 1 Post-irradiation mechanical tests of the samples display high characteristics of the strength and plasticity.
- 2 The X-ray phase analysis of the samples indicated that the irradiation caused variation of the sample phase composition as compared with the initial alloys and with those subjected to the corrosion tests without being irradiated.
- 3 The samples of the alloy “B” are characterized by lower values of penetration of sodium and zirconium into the depth of the sample compared with the alloy “A”. Decreasing of the irradiation dose acts to decrease the value of penetration of zirconium and sodium into the depth of the sample.
- 4 The irradiation of the samples acts to deteriorate their mechanical characteristics. Clarification on this phenomenon warrants further research.
- 5 The tests indicated that the fabricated alloys of the type of Hastelloy (alloy “B”) can be employed as structural materials in MSR.

This work was supported in part by the STCU,

Project #294.

#### REFERENCES

- 1.V.L. Blinkin, V.M. Novikov. *Molten-salt nuclear reactors*. Moscow: “Atomizdat”, 1978, 112 p.
- 2.V.M. Novikov, V.V. Ignatyev, V.I. Fedulov, V.N. Cherednikov. *Molten-salt nuclear power plants: prospects and problems*. Moscow: “Energoatomizdat”, 1990, 192 p.
- 3.U.R. Grims. *Problems of selection of materials for reactors with molten salts. Materials and fuel for high-temperature nuclear power plants*. Moscow: “Atomizdat”, 1966, p. 69–98.
- 4.V.M. Azhazha, A.S. Bakai, S.D. Lavrinenko, Yu.P. Bobrov, P.N. Vyugov, K.V. Kovtun, N.N. Pylpenko, V. I.Savchenko, A.D. Solopykhin, S.P. Stetzenko, D.G. Malykhin. Alloys for molten-salt reactors /*Abstract of presentation at XVI Int. Conf. On Physics of Radiation Phenomena and Radiation Materials Science, September 6-11, 2004, Alushta, the Crimea.*
- 5.V.M. Azhazha, Yu.P. Bobrov, P.N. Vyugov et al. Alloy development for fuel cycle of molten-salt reactors // *Kharkov University bulletin. Series physical “Nuclei, particles, fields”*. 2004, N 619, , issue 1(23), p. 87–94.
- 6.V.M. Azhazha, A.S. Bakai, V.A. Gurin, A.N. Dovbnya, N.V. Demidov, A.I. Zykov, E.S. Zlunytzin, S.D. Lavrinenko, L.K. Myakushko, O.A. Repikhov, A.V. Torgovkin, B.M. Shirokov, B.I. Shramenko. Radiation Test Stand for structural materials in simulation of molten-salt reactor // *Book of Abstracts, XVI Int. Conf. On Physics of Radiation Phenomena and Radiation Materials Science, September 6-11, 2004, Alushta, the Crimea*, p. 270.

7.A.S. Bakai, M.I. Bratchenko, S.V. Dyuldia. Modeling of electron beam absorption profiles in simulative experiments on radiation resistance of “Hastelloy” in fluoride melt ambience // *Book of Abstracts, XVI Int. Conf. On Physics of Radiation Phenomena and Radiation Materials Science, September 6-11, 2004, Alushta, the Crimea*, p. 274–275.

8.V.M. Azhazha, O.S. Bakai, I.V. Gurin, I.M. Neklyudov, A.O. Omel'chuk, V.V. Rozhkov, V.F. Zelenskiy, F.Garner. Study of Corrosion of Construction Materials for Reactor Employing Molten Fluoride Salts or Pb-Bi Coolant Using an Electron Irradiation Test Facility (RITF) // *Book of Abstracts, XVI Int. Conf. On Physics*

*of Radiation Phenomena and Radiation Materials Science, September 6-11, 2004, Alushta, the Crimea*, p. 8.

9.V.I. Trefilov, V.F. Moiseev. *Disperse particles in refractory metals*. Kiev: “Naukova Dumka”, 1978, 240 p.

10.I.M. Lifshitz, V.V. Slyozov // *ZhETF*. 1958, v. 35, # 2, p. 479-482.

11.K.I. Portnoy, B.N. Babich. *Dispersion-strengthened materials*. Moscow: “Metallurgy”, 1974, p. 200.

12.E.V. Collings. *Metal physics for titanium alloys*. Moscow: “Metallurgy”, 1988, p. 224.

### **ВЛИЯНИЕ ЭЛЕКТРОННОГО ОБЛУЧЕНИЯ И РАСПЛАВА ФТОРИДНЫХ СОЛЕЙ $ZrF_4 - NaF$ НА МЕХАНИЧЕСКИЕ СВОЙСТВА СПЛАВОВ ТИПА ХАСТЕЛЛОЙ Н**

***В.М. Ажажа, А.С. Бакай, А.Н. Довбня, К.В. Ковтун, С.Д. Лавриненко, Д.Г. Малыхин, Н.Н. Пилипенко, В.И. Савченко, Н.А. Семенов, С.В. Стригуновский, Б.И. Шраменко, Н. Вандерка***

В ННЦ ХФТИ выплавлены сплавы типа Хастеллой Н, которые предназначены для работы в жидкосольевых реакторах. Исследовалось совместное воздействие облучения электронами и расплава фторидов натрия и циркония при температуре 650°C в течение 700 ч на механические свойства образцов из сплавов типа Хастеллой Н.

### **ВПЛИВ ЕЛЕКТРОННОГО ОПРОМІНЕННЯ І РОЗПЛАВУ ФТОРИДНИХ СОЛЕЙ $ZrF_4 - NaF$ НА МЕХАНІЧНІ ВЛАСТИВОСТІ СПЛАВІВ ТИПУ ХАСТЕЛОЙ Н**

***В.М. Ажажа, О.С. Бакай, А.М. Довбня, К.В. Ковтун, С.Д. Лавриненко, Д.Г. Малихін, М.М. Пилипенко, В.І. Савченко, М.О. Семенов, С.В. Стригуновський, Б.І. Шраменко, Н. Вандерка***

В ННЦ ХФТИ виплавлені сплави типу Хастеллой Н, які призначені для роботи в рідинно-сольових реакторах. Досліджувалася сумісна дія опромінення електронами і розплаву фторидів натрію і цирконію при температурі 650°C протягом 700 г на механічні властивості зразків із сплавів типу Хастеллой Н.